



## Molecular Physics

An International Journal at the Interface Between Chemistry and Physics


ISSN: 0026-8976 (Print) 1362-3028 (Online) Journal homepage: <https://www.tandfonline.com/loi/tmph20>


# Quantum dynamics and spectra of the iodine atom in a strong laser field as calculated with the URIMIR package

R. Marquardt, M. Quack, J. Stohner & I. Thanopoulos

To cite this article: R. Marquardt, M. Quack, J. Stohner & I. Thanopoulos (2019): Quantum dynamics and spectra of the iodine atom in a strong laser field as calculated with the URIMIR package, Molecular Physics, DOI: [10.1080/00268976.2019.1606952](https://doi.org/10.1080/00268976.2019.1606952)

To link to this article: <https://doi.org/10.1080/00268976.2019.1606952>



 View supplementary material 

 Published online: 07 Jul 2019.

 Submit your article to this journal 

 View Crossmark data 

## Quantum dynamics and spectra of the iodine atom in a strong laser field as calculated with the URIMIR package

R. Marquardt<sup>a</sup>, M. Quack <sup>b</sup>, J. Stohner<sup>c</sup> and I. Thanopoulos <sup>d</sup>

<sup>a</sup>Laboratoire de Chimie Quantique, Institut de Chimie (UMR 7177 CNRS/Unistra), Université de Strasbourg, Strasbourg, France; <sup>b</sup>Laboratory of Physical Chemistry, ETH Zurich, Zurich, Switzerland; <sup>c</sup>ZHAW Zurich University of Applied Sciences, ICBT Institute of Chemistry and Biotechnology, ICTNS, Wädenswil, Switzerland; <sup>d</sup>Department of Optics and Optometry, T.E.I. of Western Greece, Aigio, Greece

### ABSTRACT

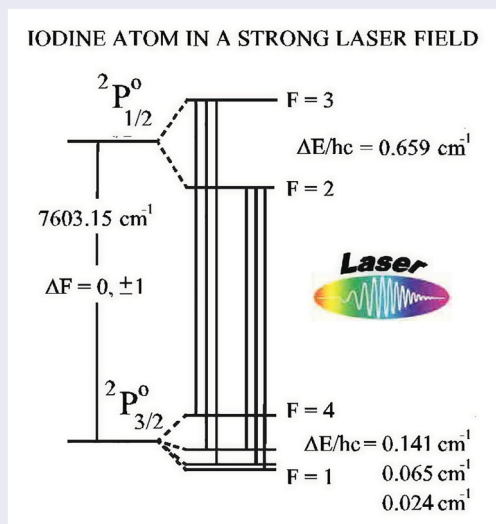
We report computations for the quantum dynamics and spectra of the iodine atom in the ground state ( $^2P_{3/2}^o$ ) subjected to a strong laser field at wavenumbers in the range of CO<sub>2</sub> laser emission. The computations include the hyperfine structure of the magnetic dipole transitions between the fine structure levels ( $^2P_{1/2}^o$  and  $^2P_{3/2}^o$ ) of the iodine atom near 7 603 cm<sup>-1</sup> important for the iodine atom laser and for the kinetic spectroscopy of iodine atoms generated in infrared multiphoton excitation and dissociation of organic iodides, where simultaneous high time and frequency resolution including hyperfine structure can be achieved, that is only limited by the Heisenberg uncertainty principle. Accurate numerical results from calculations with the URIMIR package are compared with estimates from perturbation theory and they agree well. Possibilities for experimental tests of the theoretical predictions are outlined and the URIMIR package is included in an appendix of supplementary material.

### ARTICLE HISTORY

Received 25 March 2019  
Accepted 8 April 2019

### KEYWORDS

Iodine; hyperfine structure; strong laser field; quantum dynamics; URIMIR package




## 1. Introduction

The interaction of matter and radiation leads to the 'classical', textbook like approach towards the control of atomic and molecular quantum motion [1–5]. In this context, notably Tim Softley and his group have contributed important work over several decades to the excitation and control of electronic motion in atoms,

sometimes combined also with the control of translational motion of the atoms [6–12]. Another very active area over the last few decades concerns the control of vibrational motion of polyatomic molecules by coherent infrared multiphoton excitation with the discovery of numerous important phenomena such as laser isotope separation but also considerations of mode selective

**CONTACT** M. Quack  martin@quack.ch  Physical Chemistry, ETH Zurich, CH-8093 Zurich, Switzerland

 Supplemental data for this article can be accessed here. <https://doi.org/10.1080/00268976.2019.1606952>

chemistry and the observation of vibrational preionisation of  $C_{60}$  after vibrational infrared multiphoton excitation with up to 500 photons, to provide just a small and non-exhaustive list of examples and selected reviews of the phenomena [13–26]. The theory of these processes has been well developed in parallel, as a theory of the interaction of intense coherent radiation with quantum mechanical multilevel systems, including up to very large numbers of levels, indeed, requiring quantum statistical as well as detailed quantum dynamical treatments [27–32] and early on program packages for the numerical treatment of these processes were developed, such as the URIMIR package [33] (for Unimolecular Reactions Induced by Monochromatic Infrared Radiation). Computations using these approaches concerned most importantly vibrational motion, frequently in reduced dimensional subspaces [34–38], but we can mention here also the recent implementation of the theory of coherent multiphoton excitation within the GENIUSH package enabling full-dimensional rotation-vibration-tunnelling calculations for examples such as ammonia isotopomers [39].

The present work has as focus the coherent radiative electronic excitation in the iodine atom treated as a multilevel system using the current extensions of the URIMIR package (see the Appendix). The work is motivated by considering properties of the  $^2P_{3/2}^o \leftrightarrow ^2P_{1/2}^o$  magnetic dipole transition in the ground configuration, which is among other things also the basis for the iodine atom laser [40]. This transition has been the subject of accurate measurements of the hyperfine structure and rather late also accurate determination of its absolute transition strength [41,42]. It has been used for exceptional kinetic measurements combining rates with the observation of product translational energy distributions after infrared multiphoton dissociation of organic iodides and including at the same time observation of the hyperfine distribution in the iodine atom product at what can be called ‘uncertainty limited’ kinetic measurements at highest time and energy resolution, only limited by the Heisenberg uncertainty principle [43,44]. This can be considered in some sense to be the ultimate limit of ‘kinetic spectroscopy’ as a method of time resolved spectroscopic measurement of reactants or products in reaction kinetics [45]. In these experiments involving at the same time intense  $CO_2$  laser excitation (in the wavenumber range 900–1100  $cm^{-1}$  and with intensities in the 100  $MWcm^{-2}$  range) and diode laser probing at 7600  $cm^{-1}$  with low intensity, the question of the effect of the simultaneous laser irradiations arose, in particular as far as shifts and splittings in the hyperfine spectra are concerned. These can be estimated by perturbation theory [46], but because of the usual uncontrolled uncertainties

in perturbation theory results a more fundamental theoretical test appeared to be important. We thus report here extensive numerical calculations using the extended URIMIR package, which we publish as supplementary material as well. It turns out that the perturbation theory is rather well confirmed, anticipating some of our results. We might mention here also lower resolution measurements of iodine atoms produced by photolysis of organic iodides in solid parahydrogen [47] using this fine structure transition with only partly resolved hyperfine structure.

In Section 2 of our paper, we present a brief summary of the theory of coherent excitation, in Section 3 we describe the basic features of iodine atoms in a strong laser field. Section 4 presents the computational results, complemented by summarising the conclusions in Section 5.

## 2. Theory

In this section, we review the theory of light-matter interaction and its implementation in the context of the URIMIR package [28,29]. We consider the interaction of an atomic or molecular multilevel system with a strong external electromagnetic field, e.g. a laser pulse. We treat the system within the laws of quantum mechanics and the field classically, which is a good approximation for typical conditions of intense coherent laser radiation.

### 2.1. Time evolution of a quantum mechanical state

The time evolution of a quantum mechanical state  $|\psi(t)\rangle$  is given by the evolution operator, i.e. given an initial state  $|\psi(t_0)\rangle$ , any state  $|\psi(t)\rangle$  at any time  $t$ , is given by

$$|\psi(t)\rangle = \hat{U}(t, t_0)|\psi(t_0)\rangle; \quad (1)$$

Equation (1) introduces the time evolution operator  $\hat{U}(t, t_0)$ . Since  $|\psi(t)\rangle$  obeys the Schrödinger equation, ( $i = \sqrt{-1}$ )

$$i\frac{\hbar}{2\pi} \frac{d|\psi(t)\rangle}{dt} = \hat{H}(t)|\psi(t)\rangle, \quad (2)$$

with  $\hat{H}(t)$  denoting the, in general, time-dependent Hamiltonian of the system, it follows that the operator  $\hat{U}(t, t_0)$  obeys the following differential equation [48]

$$i\frac{\hbar}{2\pi} \frac{d}{dt} \hat{U}(t, t_0) = \hat{H}(t) \hat{U}(t, t_0), \quad (3)$$

with the initial condition  $\hat{U}(t_0, t_0) = \hat{1}$ . In Equations (2) and (3),  $\hbar$  is the Planck constant.

In general, there is no simple solution of Equation (3) [48] (see, however, refs. [5,27,34,49]); under the condition of a time-independent Hamiltonian, the formal

solution of Equation (3) reads

$$\hat{U}(t, t_0) = \exp(-2\pi i \hat{H}(t - t_0)/h). \quad (4)$$

In addition, in case of a time-independent Hamiltonian it is often advantageous to use the eigenstates of  $\hat{H}$  as a basis for the representation of the state  $|\psi(t)\rangle$ . In this representation, the matrix elements  $U_{kl}(t - t_0)$  corresponding to the operator  $\hat{U}(t, t_0)$  read

$$U_{kl}(t, t_0) = \delta_{kl} \exp(-2\pi i E_k(t - t_0)/h), \quad (5)$$

with  $E_k = H_{kk}$  being the diagonal matrix element of the time-independent Hamiltonian in the same representation and  $\delta_{kl}$  denoting the Kronecker delta.  $E_k$  is the  $k$ -th eigenvalue of the matrix  $\mathbf{H}$  representing the Hamiltonian.

## 2.2. Semi-classical description of the light-matter interaction

The classical treatment of the field is justified since we study field intensities in the  $\text{MW cm}^{-2}$  to  $\text{GW cm}^{-2}$  or  $\text{TW cm}^{-2}$  region. Such intensities imply a very high number of photons per mode which is the condition for the classical treatment [50]. Furthermore, we are mainly interested in electromagnetic fields in the infrared frequency range and the dipole approximation given by the condition  $x \ll \lambda$  is used, where  $x$  is the extension of the system, and  $\lambda$  is the wavelength of the irradiation. In the infrared region,  $\lambda$  is typically larger than the extension of the atomic or molecular system by a factor of  $10^3$ , which justifies the use of the dipole approximation. Furthermore, under the intensity and frequency conditions considered here, ionisation can be neglected.

We assume now that the eigenvalues and eigenstates of the isolated multilevel system are known, i.e. the corresponding time-independent problem is already solved. We further assume a discrete energy spectrum and choose  $K$  of the eigenfunctions  $\{\chi_j(\underline{q}), j = 1 \dots K\}$  ( $\underline{q}$  stands for the complete set of generalised coordinates including all relevant degrees of freedom) for the matrix representation of the Hamilton operator of the system in interaction with a coherent monochromatic field. Keeping only the electric or magnetic dipole term in the multipole expansion of the field, the matrix elements  $H_{kl}$  are given by

$$\begin{aligned} H_{kl} &= \delta_{kl} \omega_k + f(t) \tilde{V}_{kl}^{(i)} \cos(\omega_L t + \eta) \\ &\equiv H_{kl}^0 + V_{kl}(t) \quad i = e, m \end{aligned} \quad (6)$$

with

$$\begin{aligned} \tilde{V}_{kl}^{(e)} &\equiv -\frac{2\pi \langle \chi_k | \vec{\mu}_e \cdot \vec{E}_0 | \chi_l \rangle}{h} \quad \text{or} \\ \tilde{V}_{kl}^{(m)} &\equiv -\frac{2\pi \langle \chi_k | \vec{\mu}_m \cdot \vec{B}_0 | \chi_l \rangle}{h} \end{aligned} \quad (7)$$

where  $\vec{\mu}_i$ , ( $i = e, m$ ) is the electric or magnetic dipole operator of the multilevel system depending on what might dominate the interaction,  $\omega_k = 2\pi E_k/h$  is the  $k$ -th eigenvalue of the time-independent Hamiltonian  $\mathbf{H}^0$  (in units of angular frequency),  $f(t)$  is the pulse shape function of the irradiation,  $\omega_L$  is the angular frequency of the laser field,  $\eta$  is a time independent phase factor and  $\vec{E}_0$  is the vector valued amplitude of the electric field and  $\vec{B}_0$  is the vector valued amplitude of the magnetic induction. The dipole approximation allows us to consider  $\vec{E}_0$  or  $\vec{B}_0$  to be constant over the spatial dimensions of the system. Decay phenomena can be further taken into account in a phenomenological way by introducing complex eigenfrequencies [48,49],  $\omega'_k = \omega_k - i\gamma_k/2$ , where  $\gamma_k$  equals the inverse of the lifetime of the unstable  $k$ -th state (in units of angular frequency) [28,51]. When the electric dipole matrix elements  $\tilde{V}_{kl}^e$  vanish due to symmetry reasons, magnetic dipole matrix elements or matrix elements due to higher terms in the multipole expansion of the electromagnetic field should be considered, as it is the case for the iodine atom discussed below. According to the parity selection rule the electric dipole coupling connects only states of different parity, whereas the magnetic dipole coupling connects only states of the same parity when considering only the parity conserving electromagnetic interactions [52].

By using  $\hat{H}^0 \chi_m = \omega_m \chi_m$ , the wave function  $\psi(t)$  of the system can be written

$$\psi(t) = \sum_{k=1}^K b_k(t) \chi_k \quad (8)$$

In this particular representation, Equation (1) takes the form (with the time evolution matrix  $\mathbf{U}$  in the same representation)

$$\mathbf{b}(t) = \mathbf{U}(t, t_0) \mathbf{b}(t_0) \quad (9)$$

while the Schrödinger equation reads

$$i\dot{\mathbf{b}}(t) = \mathbf{H} \mathbf{b}(t) \quad (10)$$

with  $\mathbf{b}(t) = (b_1(t), b_2(t), \dots, b_L(t))^T$  (T for transpose) and  $\mathbf{H}$  defined by Equation (6).

The Hamiltonian given by Equation (6) depends explicitly on time. Thus, it is not possible to use the formal solution of Equation (4) for calculating the evolution operator. Since only very few solutions of Equation (3) with the Hamiltonian of Equation (6) are known at present, several approximations have been introduced in order to compute  $\mathbf{U}(t, t_0)$  numerically. We refer to [1–5,27–29] for different approaches on dealing with the interaction between a multilevel system and a strong electromagnetic field. In our investigations, we

concentrate on two particular approximations, the Floquet approximation and the weak-field quasi-resonant approximation (QRA), which we present in detail now.

### 2.3. The Floquet approximation (FA)

Taking advantage of the periodicity in the Hamiltonian given by Equation (6), one can numerically integrate Equation (3) for one period  $\tau = 2\pi/\omega_L$  and obtain  $\hat{U}(\tau + t_0, t_0)$ . At any subsequent time  $t = m \cdot \tau$ , which is an integer multiple of  $\tau$ ,  $|\psi(t)\rangle$  can be calculated by

$$|\psi(t)\rangle = \left[ \hat{U}(\tau + t_0, t_0) \right]^m |\psi(t_0)\rangle \quad (11)$$

This approach is also applicable for  $t = m \cdot \tau + \Delta t$ , with  $\tau > \Delta t > 0$ . In this case,  $\hat{U}(\Delta t + t_0, t_0)$  is additionally needed so that

$$|\psi(t)\rangle = \hat{U}(\Delta t + t_0, t_0) \left[ \hat{U}(\tau + t_0, t_0) \right]^m |\psi(t_0)\rangle \quad (12)$$

The theoretical foundation of this approach is the classical theorem by Floquet [53,54], which when applied to our case [27–29] states that for a Hamiltonian with period  $\tau$

$$\hat{H}(t) = \hat{H}(t + \tau), \quad \forall t \quad (13)$$

$\hat{F}(t, t_0)$  and  $\hat{A}(t)$  exist so that the evolution operator  $\hat{U}$  satisfies the following equations

$$\hat{U}(t, t_0) = \hat{F}(t, t_0) \exp\left(\hat{A}(t - t_0)\right) \quad (14)$$

$$\hat{F}(t_0, t_0) = \hat{1} \quad (15)$$

$$\hat{F}(t + n\tau, t_0) = \hat{F}(t, t_0) \quad (16)$$

$$\hat{A}(t') = \hat{A}(t''), \quad \forall t', t'' \quad (17)$$

Within the Floquet approximation (sometimes also called Floquet-Liapunoff-approximation), matrix representations  $\mathbf{F}(t_0 + \tau, t_0)$  and  $\mathbf{A}(t)$  are obtained by numerical integration over  $\tau$ . However, two practical aspects define the limitations of this approximative method. First, a system of coupled complex differential equations can hardly be solved completely for very large systems, i.e. systems of the order of millions of states, or even larger. Secondly, the diagonalisation of the complex evolution matrix in such cases for further use in Equations (11)–(12) can introduce significant numerical errors.

### 2.4. The weak-field Quasi-Resonant Approximation (QRA)

As mentioned above, the explicit time dependence in Equation (6) prohibits the direct application of

Equation (4). In order to overcome this difficulty, the quasi-resonant approximation which is a generalisation of the rotating-wave approximation (RWA) for a two level system to multilevel systems has been introduced [27,28]. The main idea is to transform the Hamiltonian given by Equation (6) into such a form that within a reasonable approximation the explicit time dependence can be removed. The following steps summarise the procedure and we refer to ref. [29] for further discussion:

- (1) Since only one electromagnetic field is considered here, we can choose  $\eta = 0$  without any loss of generality and write

$$\cos(\omega_L t) = \frac{1}{2} \left[ \exp(i(\omega_L t)) + \exp(-i(\omega_L t)) \right] \quad (18)$$

- (2) We introduce an integer level quantum number  $n_k$  for each energy level by writing

$$\omega_k = n_k \cdot \omega_L + X_k \cdot \omega_L \quad (19)$$

with  $X_k \in (-\frac{1}{2}, \frac{1}{2})$ . We now transform from the ‘spectroscopic basis’, i.e. the state vector  $\mathbf{b}$  formulated in the basis of eigenstates, as given in Equation (10), into a state vector  $\mathbf{a}$ , formulated in the ‘quasiresonant basis’ and defined by

$$\mathbf{a} \equiv \mathbf{S} \mathbf{b}, \quad (20)$$

where  $\mathbf{S}$  is a diagonal matrix given by

$$S_{kk} \equiv \exp(in_k \omega_L t). \quad (21)$$

- (3) We consider the case where the two following conditions are fulfilled for any two arbitrary states  $n$  and  $m$

$$|\tilde{V}_{nm}| \ll \omega_L \quad \text{‘weak field’} \quad (22)$$

$$|D_{nm}| \equiv |\omega_n - \omega_m - \omega_L \cdot \text{sgn}(\omega_n - \omega_m)| \ll \omega_L \quad \text{‘quasi-resonant’} \quad (23)$$

While the first condition can always be satisfied, e.g. by decreasing the intensity of the electromagnetic field, the second condition is system dependent.

- (4) We drop the high frequency part of the Hamiltonian which is proportional to  $\exp(-i(\omega_L t))$  with a similar reasoning as for the RWA of the two-level problem [27,50]. For an index pair  $jk$ , with  $j < k$ , it then follows

$$H_{jk} \sim \exp\left(i(-X_j \cdot \omega_L + \omega_j + \omega_L - \omega_k + X_k \cdot \omega_L)\right) \quad (24)$$

- (5) If

$$|n_j - n_k| = 1 \quad (25)$$



is valid, all terms of the Hamiltonian including such combinations of indices are time independent. We thus neglect all terms that include combinations of indices with

$$|n_j - n_k| \neq 1 \quad (26)$$

because for such far off-resonant levels the sum of many fast oscillating interaction terms nearly cancels out and the effective interaction becomes small compared to the interaction between resonant levels.

- (6) We end up with a time independent effective Hamiltonian within the QRA, in the matrix representation  $H^{\text{QRA}}$  given by

$$H_{jk}^{\text{QRA}} = \delta_{jk} \cdot X_k \cdot \omega_L + \frac{1}{2} \tilde{V}_{jk} \quad (27)$$

After diagonalising  $H^{\text{QRA}}$  the evolution of the system is calculated according to Equations (5) and (9). The justification of the above approximations in the domain of infrared laser chemistry has been the subject of many studies (see [23] and references therein). It is found to be valid to good approximation, often well beyond the conditions specified by Equations (22) and (23) [32,34,36].

## 2.5. Physical quantities of interest

Below we present some physical quantities of interest within the URIMIR package, but firstly we give two useful equations for calculating the electric and magnetic dipole coupling matrix elements under linearly polarised laser fields according to Equation (7)

$$\frac{\tilde{V}_{kl}^{(e)}}{2\pi c} \cong -4.609\,277 \cdot 10^{-4} \frac{M_{kl}^{(e)}}{D} \sqrt{\frac{I}{W\text{cm}^{-2}}} \quad \text{cm}^{-1} \quad (28)$$

and

$$\frac{\tilde{V}_{kl}^{(m)}}{2\pi c} \cong -4.274\,648 \cdot 10^{-6} \frac{M_{kl}^{(m)}}{\mu_b} \sqrt{\frac{I}{W\text{cm}^{-2}}} \quad \text{cm}^{-1} \quad (29)$$

where  $M_{kl}^{(i)}$  stands for the electric ( $i = e$ ) or magnetic ( $i = m$ ) transition dipole moment between the  $k$ -th and  $l$ -th eigenstates. We note that  $1\text{ D} \approx 0.393\,43\, e\, a_0$  and  $1\, \mu_b/c_0 = \alpha\, a_0/2$ , with  $\mu_b$  being the Bohr magneton and  $\alpha$  being the fine structure constant [55]. We note that in the actual program used for the calculations of the data presented in the results section, the numerical value presented in Equation (28) was defined as  $4.609\,273\,676\, 10^{-4}$ , which was derived from an older definition of the Planck constant. If the numerical value from Equation (28) is used, some numerical values presented in the results section might change in the 6th decimal place.

An operator which we often consider in our studies is the density operator  $\hat{\rho}$  of the system given by a matrix representation

$$P_{jk}^{(c)}(t) = c_j(t)c_k^*(t), \quad (30)$$

where  $\mathbf{c}$  is the state vector representation in an arbitrary basis. We often use the quasis resonant basis, i.e.  $P_{jk}^{(a)}(t) = a_j(t)a_k^*(t)$ , in our computations, while the density matrix in the spectroscopic basis is given by  $P_{jk}^{(b)}(t) = b_j(t)b_k^*(t)$ . The transformation of  $\mathbf{P}$  between these two basis representations reads

$$\mathbf{P}^{(b)} = \mathbf{S}^\dagger \mathbf{P}^{(a)} \mathbf{S} \quad (31)$$

with  $\mathbf{S}$  defined by Equation (21). If the initial value  $\hat{\rho}(t_0)$  is known, then  $\hat{\rho}(t)$  can be calculated in the Schrödinger picture by

$$\hat{\rho}(t) = \hat{U}(t, t_0)\hat{\rho}(t_0)\hat{U}^\dagger(t, t_0); \quad (32)$$

Equation (32) is known as the Liouville-von Neumann equation [56] in its integrated form, and similar equations are valid for any of its matrix representations.

Further physical quantities of importance in quantum dynamical investigations are the expectation value of the absorbed energy of the system  $E_{\text{abs}}(t)$  and its time average  $\langle E_{\text{abs}} \rangle_T$  given by

$$E_{\text{abs}}(t) = \sum_i (P_i(t) - P_i(t_0))E_i \quad (33)$$

$$\langle E_{\text{abs}} \rangle_T \equiv \lim_{T \rightarrow \infty} \frac{1}{T} \int_{t_0}^T E_{\text{abs}}(t) dt, \quad (34)$$

where the summation  $i$  runs over all energy levels  $E_i$  of the system considered.  $P_i(t) = P_{ii}^{(b)}(t) = b_i(t)b_i^*(t)$  stands for the total population of level  $i$  of the isolated Hamiltonian. More physical quantities of specific interest to the investigations on the iodine atom presented here will be introduced below.

## 3. The iodine atom in a strong laser field

In this section, we study the influence exerted by a strong off-resonant laser field on the position of the  ${}^2P_{3/2}^\circ(F=4) \rightarrow {}^2P_{1/2}^\circ(F=3)$  magnetic dipole induced hyperfine transition at  $7603.138\text{ cm}^{-1}$  in the ground term of atomic iodine. In order to study the interaction between the strong laser field and the iodine atom, we calculate the position of the  ${}^2P_{3/2}^\circ(F=4) \rightarrow {}^2P_{1/2}^\circ(F=3)$  transition when the strong electromagnetic field couples to the atomic energy levels of iodine due to magnetic and electric dipole interactions. The ground electronic term  ${}^2P$

has odd (negative) parity, which is also the total parity of the atom, as the iodine nucleus  $^{127}\text{I}$  has even (positive) parity.

### 3.1. Spectroscopic data of the physical problem

We consider an iodine atom interacting with two linearly polarised CW laser fields. One laser off-resonant at  $1086\text{ cm}^{-1}$  with  $750\text{ MWcm}^{-2}$  intensity and a second weak near-resonant laser, which probes the  ${}^2\text{P}_{3/2}^{\circ}(F=4) \rightarrow {}^2\text{P}_{1/2}^{\circ}(F=3)$  transition. We study the cases when the probe field is  $10^4$  and  $10^7$  times weaker than the off-resonant field.

The following assumptions considering the interaction of the iodine atom with each irradiation field are further made in our model: (a) the hyperfine levels of the odd parity ground term couple to each other in the presence of a laser field mainly due to magnetic dipole interaction, since the parity selection rule forbids electric dipole coupling in the ground term. All higher multipole interactions are significantly weaker and are neglected in our considerations. Indeed, the electric quadrupole contribution has been estimated to be only 0.7% of the magnetic dipole contribution [42]. (b) Iodine electronically excited states beyond the ground state are considered; they couple directly to the ground  ${}^2\text{P}_{3/2}^{\circ}$  and  ${}^2\text{P}_{1/2}^{\circ}$  terms. The leading interaction in such cases is of electric dipole type, which implies that only excited states with even parity are considered. Although all excited states of the same parity couple to each other due to magnetic and higher multipole interactions, we neglect these couplings

since such interactions are much weaker than those of electric dipole type with the ground term states. Thus, in short, in our model only magnetic dipole coupling between the hyperfine levels of the ground terms and electric dipole coupling between the hyperfine levels of even parity excited states and the hyperfine levels of the odd parity ground terms are considered.

The coupling matrix elements between the excited states and the ground level can be derived, when the Einstein coefficient and the wavenumber for the corresponding transition are known. We use experimentally known spectroscopic data. In our study, we include excited states of even parity from the literature, for which the Einstein coefficient for transitions to the ground term is known. Since we are interested in the shift of a transition between the hyperfine levels of the ground term, it is desirable to have experimental information of the hyperfine structure of all excited states considered. Unfortunately, experimental data on the hyperfine structure are available only for some of these excited states. Table 1 below shows all atomic states considered, as well as their hyperfine structure as far as known. We note the two different notations used for classifying the excited states. The last four configurations in Table 1 are given in the  $[J]\ell$  coupling scheme classification of Minnhagen [57], while all others are given in a  $LS$  coupling scheme classification. The  $[J]\ell$  coupling scheme is appropriate, when electronic configurations containing one strongly excited electron are considered, while it is assumed that its orbital angular momentum  $\ell$  is conserved ('good quantum number'), as well as the total angular momentum  $J$  of the atomic core.

**Table 1.** Electronic states of atomic iodine included in our calculations, their excitation energy with respect to the ground level and the energy difference between two successive hyperfine levels of a given term. The terms 1–10 are given in the  $LS$  coupling scheme. The terms 11–14 are given in the  $[J]\ell$  coupling scheme according to ref. [57]. The notation is explained in the text.

$N_0$	Term	Parity	Energy / (hc cm $^{-1}$ )	Hyperfine splitting / $10^{-3}\text{ cm}^{-1}$					Ref.
				(5,4)	(4,3)	(3,2)	(2,1)	(1,0)	
1	$5p(5) {}^2\text{P}_{3/2}^{\circ}$	odd	0.0		141	66	24		[42]
2	$5p(5) {}^2\text{P}_{1/2}^{\circ}$	odd	7 603.15 <sup>a</sup>			659			[42]
3	$5p(4)({}^3\text{P})6s {}^2\text{P}_{3/2}$	even	56 092.88 <sup>a</sup>		100	65	39		[58]
4	$5p(4)({}^3\text{P})6s {}^2\text{P}_{1/2}$	even	63 186.76 <sup>a</sup>			159			[59]
5	$5p(4)({}^3\text{P})6s {}^4\text{P}_{5/2}$	even	54 633.46 <sup>a</sup>	215	191	155	109	56	[58]
6	$5p(4)({}^3\text{P})6s {}^4\text{P}_{1/2}$	even	60 896.27 <sup>a</sup>			216			[58]
7	$5p(4)({}^3\text{P})6s {}^4\text{P}_{3/2}$	even	61 819.81 <sup>a</sup>		61	61	49		[58]
8	$5p(4)({}^1\text{D})6s {}^2\text{D}_{5/2}$	even	66 020.24 <sup>c</sup>						
9	$5p(4)({}^1\text{D})6s {}^2\text{D}_{3/2}$	even	66 355.21 <sup>c</sup>						
10	$5p(4)({}^1\text{S})6s {}^2\text{S}_{1/2}$	even	70 354.93 <sup>c</sup>						
11	$5p(4)({}^3\text{P}_2)5d [2]_{5/2}$	even	70 150.82 <sup>b</sup>						
12	$5p(4)({}^3\text{P}_2)5d [2]_{3/2}$	even	70 353.17 <sup>b</sup>						
13	$5p(4)({}^3\text{P}_2)5d [0]_{1/2}$	even	68 956.52 <sup>b</sup>						
14	$5p(4)({}^3\text{P}_2)6d [1]_{3/2}$	even	76 138.50 <sup>b</sup>						

<sup>a</sup> Energy of the term of the electronic configuration according to [60]. Since the hyperfine structure for a given term is neglected, it is reasonable to assume that the energy refers to the weighted mean of the energies of the hyperfine levels of the term, which is called the centre of gravity of the term in analogy to the case of fine structure [61].

<sup>b</sup> according to [62]. No hyperfine structure experimentally known.

<sup>c</sup>as<sup>a</sup>. No hyperfine structure experimentally known.

The energy of each hyperfine level in the  ${}^2P^\circ$  ground term (levels 1 and 2 in Table 1) is calculated with help of Table 2 of ref. [42], in which the experimental transition wavenumbers between the hyperfine levels are given, and the level structure of atomic iodine as shown in Figure 1; the  ${}^2P_{3/2}^\circ(F=1)$  level has zero energy by definition. For each further term, for which the hyperfine structure is known, the energy of each hyperfine level can be calculated easily with help of Table 1; we outline the method on the example of the seventh term of Table 1: Assuming that  $x$  is the energy difference expressed in terms of the wavenumber in  $\text{cm}^{-1}$  between the lowest hyperfine level  $F=1$  and the centre of gravity of the term, which is the weighted mean of the energies of the hyperfine levels of the term, then the energy difference between the level  $F=2$  and the centre of gravity equals  $x-49$ , for  $F=3$  it equals  $x-49-61$  and for  $F=4$  it equals  $x-171$ . By definition of the centre of gravity, the following equality is valid:  $3 * x + 5 * (x - 49) + 7 * (x - 110) + 9 * (x - 171) = 0$ , where 3,5,7,9 denote the number of energetically degenerate states in levels with  $F=1, F=2, F=3$  and  $F=4$ , respectively. By solving for  $x$ , the energy of the lowest hyperfine level can be obtained and consequently the energy for all hyperfine levels of the term. For all terms, for which no hyperfine structure is known, we assume that the corresponding hyperfine levels are energetically degenerate. The influence of this approximation on the results is insignificant, since test calculations, where random hyperfine splittings of the same order of

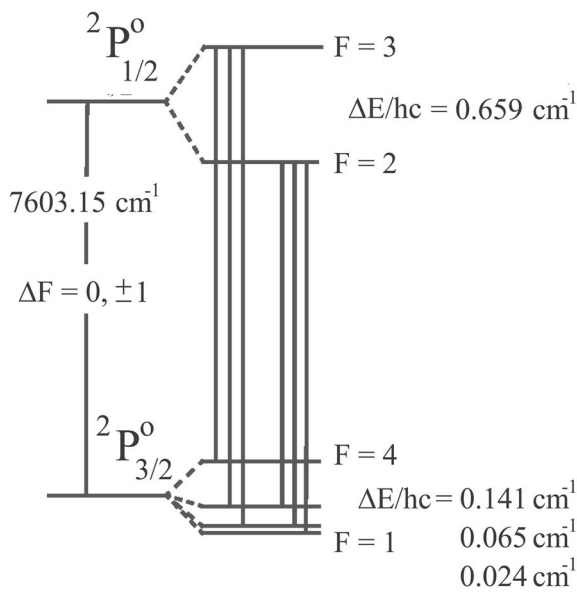


**Figure 1.** The fine and hyperfine structure in the  ${}^2P$  term of the  $5p(5)$  ground configuration of atomic iodine [41]. Solid lines denote the magnetic dipole allowed  $\Delta F = 0, \pm 1$  transitions between the hyperfine levels [41–44]. The  $\Delta E$  gives the values for the energy differences between the adjacent levels as indicated.

magnitude as experimental splittings of terms have been introduced, for which the hyperfine structure is known, give similar results to the results assuming that the hyperfine levels are energetically degenerate. In Table 2, the Einstein coefficients  $A$  and the corresponding transition wavenumbers  $\tilde{\nu}$  between the atomic terms considered are given.

In order to calculate the coupling matrix elements for the transitions considered, we use the information obtained from experimental values of the corresponding Einstein coefficients. For consistency values for both type of transitions are taken from the same reference. The following useful identity from ref. [46] is used in order to calculate reduced matrix elements:

$$\sum_{FF'} \sum_{mm'} |\langle \Phi J F m | \hat{O}_k | \Phi' J' F' m' \rangle|^2 = \frac{1}{3} (2I + 1) |\langle \Phi J || \hat{O} || \Phi' J' \rangle|^2 \quad (35)$$

where  $\hat{O}$  is either the electric or the magnetic dipole operator,  $\hat{O}_k$  stands for its  $k$ -th cartesian component and  $I$  is the nuclear spin of atomic iodine.

The reduced matrix elements  $M^{(m)}$  for magnetic and  $M^{(e)}$  for electric dipole induced transitions are then given by the following equations, in which the Gaussian system of electromagnetism is adopted (see ref. [64] for conversion to the SI system of units). For the magnetic dipole interaction in the  ${}^2P^\circ$  ground term, we use

$$|M^{(m)}|^2 ({}^2P_{3/2}^\circ, {}^2P_{1/2}^\circ) \equiv |\langle {}^2P_{3/2}^\circ || \hat{m}^1 || {}^2P_{1/2}^\circ \rangle|^2 = 2 \frac{3h}{64\pi^4} \frac{1}{\tilde{\nu}^3} A \quad (36)$$

where  $\tilde{\nu}$  stands for the transition wavenumber,  $\hat{m}^1$  is the magnetic dipole operator and  $A$  is the corresponding Einstein coefficient. For the electric dipole interaction between the electronic configurations  $\Phi_i$  and  $\Phi_j$  we use

$$|M^{(e)}|^2 (\Phi_i, \Phi_j) \equiv |\langle \Phi_i || \hat{e}^1 || \Phi_j \rangle|^2 = g_j \frac{3h}{64\pi^4} \frac{1}{\tilde{\nu}^3} A \quad (37)$$

where  $g_j$  stands for the degeneracy of the upper level  $j$ ,  $\hat{e}^1$  is the electric dipole operator,  $A$  is the corresponding Einstein coefficient and  $\tilde{\nu}$  stands for the transition wavenumber.

Consider a magnetic dipole moment of  $1 \mu_B$ . In the Gaussian system of units, the magnetic dipole moment becomes  $1 \mu_B / c_0 = 1 (\alpha/2) e a_0$ . In the Gaussian system of units a magnetic dipole transition induced by a magnetic dipole moment of  $1 \mu_B$  can thus be considered as an electric dipole transition induced by an electric dipole moment of  $1 e a_0$ , just weakened by the numerical factor  $\alpha/2$ . Because in the Gaussian system of units



**Table 2.** Experimentally known Einstein coefficients  $A$  and the corresponding wavenumbers  $\tilde{\nu}$  for transitions in atomic iodine, as well as the type of the dominant electromagnetic multipole interaction, which induces the transition.

	type of inter.	transition	$A / s^{-1}$	$\tilde{\nu}^a / cm^{-1}$	Ref.
1	magnetic dipole	$5p(5) \ ^2P_{1/2}^\circ - 5p(5) \ ^2P_{3/2}^\circ$	$6.95 \cdot 10^0$	7 603.15	[42]
2	electric dipole	$5p(4) \ (^3P)6s \ ^4P_{1/2} - 5p(5) \ ^2P_{1/2}^\circ$	$287 \cdot 10^4$	53 304.90	[63]
3	electric dipole	$5p(4) \ (^3P)6s \ ^4P_{1/2} - 5p(5) \ ^2P_{3/2}^\circ$	$370 \cdot 10^5$	60 901.34	[63]
4	electric dipole	$5p(4) \ (^3P)6s \ ^4P_{5/2} - 5p(5) \ ^2P_{3/2}^\circ$	$160 \cdot 10^5$	54 644.81	[63]
5	electric dipole	$5p(4) \ (^3P)6s \ ^4P_{3/2} - 5p(5) \ ^2P_{3/2}^\circ$	$271 \cdot 10^6$	56 085.25	[63]
6	electric dipole	$5p(4) \ (^3P)6s \ ^4P_{3/2} - 5p(5) \ ^2P_{1/2}^\circ$	$296 \cdot 10^4$	48 496.60	[63]
7	electric dipole	$5p(4) \ (^3P)6s \ ^2P_{1/2} - 5p(5) \ ^2P_{1/2}^\circ$	$211 \cdot 10^6$	55 586.44	[63]
8	electric dipole	$5p(4) \ (^3P)6s \ ^2P_{1/2} - 5p(5) \ ^2P_{3/2}^\circ$	$207 \cdot 10^6$	63 171.19	[63]
9	electric dipole	$5p(4) \ (^3P)6s \ ^2P_{3/2} - 5p(5) \ ^2P_{3/2}^\circ$	$134 \cdot 10^6$	61 804.68	[63]
10	electric dipole	$5p(4) \ (^3P)6s \ ^2P_{3/2} - 5p(5) \ ^2P_{1/2}^\circ$	$692 \cdot 10^4$	54 200.54	[63]
11	electric dipole	$5p(4) \ (^1D)6s \ ^2D_{5/2} - 5p(5) \ ^2P_{3/2}^\circ$	$205 \cdot 10^6$	66 006.60	[63]
12	electric dipole	$5p(4) \ (^1D)6s \ ^2D_{3/2} - 5p(5) \ ^2P_{3/2}^\circ$	$175 \cdot 10^5$	66 357.00	[63]
13	electric dipole	$5p(4) \ (^1D)6s \ ^2D_{3/2} - 5p(5) \ ^2P_{1/2}^\circ$	$205 \cdot 10^6$	58 754.41	[63]
14	electric dipole	$5p(4) \ (^1S)6s \ ^2S_{1/2} - 5p(5) \ ^2P_{3/2}^\circ$	$138 \cdot 10^4$	70 372.98	[63]
15	electric dipole	$5p(4) \ (^1S)6s \ ^2S_{1/2} - 5p(5) \ ^2P_{1/2}^\circ$	$114 \cdot 10^6$	62 735.26	[63]
16	electric dipole	$5p(4) \ (^3P_2)5d[0]_{1/2} - 5p(5) \ ^2P_{3/2}^\circ$	$55 \cdot 10^6$	68 965.52	[62]
17	electric dipole	$5p(4) \ (^3P_2)5d[1]_{3/2} - 5p(5) \ ^2P_{1/2}^\circ$	$74 \cdot 10^6$	68 535.40	[62]
18	electric dipole	$5p(4) \ (^3P_2)5d[2]_{5/2} - 5p(5) \ ^2P_{3/2}^\circ$	$120 \cdot 10^6$	70 150.82	[62]
19	electric dipole	$5p(4) \ (^3P_2)5d[2]_{3/2} - 5p(5) \ ^2P_{3/2}^\circ$	$97 \cdot 10^6$	70 353.17	[62]

<sup>a</sup>  $\tilde{\nu}$  of the transition as given in the corresponding reference.

the electric field and the magnetic induction field have the same units, one can thus numerically treat magnetic dipole transitions as electric dipole transitions by including the  $\alpha/2$  numerical factor in the value of the magnetic dipole matrix element. In such a case, and for a given laser intensity, the value of the  $\vec{E}$  field instead of the value of the  $\vec{B}$  field is used in the numerical treatment; we however stress that the symmetry rules related to magnetic dipole transitions must be taken into account explicitly in the definition of the coupling matrix elements between the levels included in the numerical simulation.

The states included in our calculations are denoted by  $|\Phi_i J_i F_i m_{F_i}\rangle$ , where  $\Phi_i$  stands for the  $i$ -th electronic configuration considered,  $J_i$  is the total electronic angular momentum,  $F_i \equiv J_i + I$  is the total angular momentum resulting by coupling the electronic angular momentum  $J_i$  to the nuclear spin of iodine  $^{127}\text{I} = 5/2$  and  $m_{F_i}$  is the magnetic quantum number. The matrix elements for magnetic dipole transitions are given by

$$\begin{aligned}
 \langle {}^2P^\circ \frac{3}{2} F m_F | \hat{m}_z^1 | {}^2P^\circ \frac{1}{2} F' m_{F'} \rangle &= (-1)^{F-m_F} \begin{pmatrix} F & 1 & F' \\ -m_F & 0 & m_{F'} \end{pmatrix} \\
 &\times (-1)^{F'+4} \sqrt{2F'+1} \\
 &\times \sqrt{2F'+1} \begin{Bmatrix} \frac{3}{2} & F & \frac{5}{2} \\ F' & \frac{1}{2} & 1 \end{Bmatrix} \\
 &\times M^{(m)} ({}^2P_{3/2}^\circ, {}^2P_{1/2}^\circ)
 \end{aligned} \quad (38)$$

The matrix elements for electric dipole transitions are given by

$$\begin{aligned}
 \langle \Phi_i J_i F_i m_{F_i} | \hat{e}_z^1 | \Phi_j J_j F_j m_{F_j} \rangle &= (-1)^{F_i - m_{F_i}} \begin{pmatrix} F_i & 1 & F_j \\ -m_{F_i} & 0 & m_{F_j} \end{pmatrix} \\
 &\times (-1)^{F_j + J_j + \frac{7}{2}} \sqrt{2F_i + 1} \\
 &\times \sqrt{2F_j + 1} \begin{Bmatrix} J_i & F_j & \frac{5}{2} \\ F_i & J_j & 1 \end{Bmatrix} \\
 &\times M^{(e)} (\Phi_i, \Phi_j)
 \end{aligned} \quad (39)$$

The symbols in parentheses and curly brackets are the Wigner  $3j$  and  $6j$ -symbols, respectively. They are discussed in refs. [65,66]). Since a static external magnetic field removes the degeneracy of states with respect to the magnetic quantum number  $m_F$  (Zeeman effect) due to non vanishing diagonal matrix elements for the magnetic dipole operator, such matrix elements for the  ${}^2P^\circ$  ground term within  $LS$  coupling are given by

$$\begin{aligned}
 \langle {}^2P^\circ J F m_F | \hat{m}_z^1 | {}^2P^\circ J F m_F \rangle &= \left( 1 + \frac{J(J+1) - L(L+1) + S(S+1)}{2J(J+1)} \right) \\
 &\times \frac{F(F+1) + J(J+1) - I(I+1)}{2F(F+1)} m_F \frac{\mu_b}{c_0}
 \end{aligned} \quad (40)$$

in the Gaussian system of units. Although only periodic time-dependent electromagnetic fields are considered in our study, for which no Zeeman effect is expected, we

include such diagonal matrix elements in order to be complete in our treatment. Indeed, no Zeeman effect for the states of the ground term has been observed in the numerical calculations with periodic fields, while test calculations with static fields showed the expected Zeeman splitting. In order to compute all matrix elements necessary in our calculations, all  $3j$  and  $6j$  symbols have been calculated with the computer codes given in [65].

Decay phenomena of the excited states due to spontaneous emission can be taken in account in a phenomenological way by introducing complex energy eigenvalues. Since in our approach units of angular frequency are used, such complex terms are denoted by  $\omega'_l \equiv \omega_l - i\gamma_l/2$ , where  $\omega_l$  is the angular frequency corresponding to the real energy eigenvalue of the state  $l$  and  $\gamma_l$  is the total Einstein coefficient of the transition from  $l$  to all lower terms, also in units of angular frequency [51].

### 3.2. Treatment within perturbation theory

Only the strong off-resonant laser field is considered and according to second order perturbation theory [46] the mean energy shift  $\Delta\bar{E}_k$  of the eigenvalue  $E_k$  of the  $k$ -th state is given by

$$\Delta\bar{E}_k = \frac{2\pi}{h} \sum_{l \neq k} \frac{\omega_{kl} \tilde{V}_{kl}^2}{\omega_{kl}^2 - \omega_s^2} (E_s^z)^2 \quad (41)$$

where the summation is over all states included except state  $k$ .  $\tilde{V}_{kl}$  is the coupling matrix element between state  $k$  and  $l$ ,  $E_s^z$  is the electric field strength amplitude of the strong electromagnetic field (it is assumed that it is  $z$ -polarised),  $\omega_s$  is the angular frequency of the field, and  $\omega_{kl} \equiv 2\pi(E_k - E_l)/h$  is the angular frequency of the transition between states  $k$  and  $l$ . The transition angular frequency between states  $k$  and  $l$  under the influence of the field  $\omega_{kl}^{\text{field}}$  can thus be calculated by

$$\omega_{kl}^{\text{field}} \equiv \omega_{kl} + \frac{2\pi(\Delta\bar{E}_k - \Delta\bar{E}_l)}{h} \quad (42)$$

### 3.3. Numerical integration of the time-dependent Schrödinger equation

As mentioned above, we include the  $\alpha/2$  factor in the numerical value of all magnetic dipole matrix elements and treat them as of electric dipole type in the numerical simulation. Therefore, there is formally no  $\vec{B}$  field in the Hamilton operator used; its matrix representation is given by

$$H_{kl} = \frac{h}{2\pi} \delta_{kl} \omega_{kl} - \tilde{V}_{kl}^{\text{strong}} \cos(\omega_s \cdot t) - \tilde{V}_{kl}^{\text{weak}} \cos(\omega_w \cdot t + \eta) \quad (43)$$

where  $\omega_{kl}$  was defined in relation with Equation (42) and can be a complex number, if decay phenomena are phenomenologically included,  $\omega_s$  is the angular frequency of the strong field,  $\omega_w$  is the angular frequency of the weak probe field,  $\eta$  is the phase factor between the two fields and  $\tilde{V}_{kl}^{\text{strong/weak}}$  is the coupling matrix element between states  $k$  and  $l$  for the strong and weak fields, respectively, in units of angular frequency. In general,  $\eta = 0$  is used, since comparison with the results of test calculations with  $\eta \neq 0$  has shown that the results do not depend on the choice of  $\eta$ .

We use the Floquet approximation in order to numerically integrate the time-dependent Schrödinger equation. The Floquet approximation is applicable only on periodic Hamilton operators. In order to enforce periodicity in Equation (43), we demand  $\omega_s = \omega_w/7$ , which implies that a strong field at  $1\,086.162\text{ cm}^{-1}$  is considered, since the transition under study occurs at  $7\,603.138\text{ cm}^{-1}$ . This choice gives a wavenumber for the strong field, which is the closest to the experimental conditions. The necessary periodicity of the Hamiltonian implies that in order to calculate the time averaged absorbed energy of the system as a function of the angular frequency of the resonant field  $\omega_w$  (or correspondingly  $\tilde{\nu}_w$ ), the angular frequency of the off-resonant field  $\omega_s$  (or correspondingly  $\tilde{\nu}_s$ ) must also vary. In our calculations  $\tilde{\nu}_w$  varies over the range of  $7\,603.14 \pm 0.02\text{ cm}^{-1}$ ; consequently  $\tilde{\nu}_s$  takes values over the range of  $1\,086.162 \pm 0.003\text{ cm}^{-1}$ . This is close to the two CO<sub>2</sub> laser lines near  $1086\text{ cm}^{-1}$ . By demanding  $\omega_s = \omega_w/7$ , the Hamiltonian in Equation (43) is periodic with period  $\tau = 2\pi/\omega_s$ , which is about 30 fs.

The position and line shape of the transition under study are calculated by computing the time averaged absorbed energy spectrum, according to Equation (34), for the Hamilton operator defined by Equation (43) within the Floquet approximation. The initial condition is always chosen such that only the states of the hyperfine structure of the  $^2\text{P}_{3/2}^{\circ}$  configuration are populated corresponding to their statistical weights. In Equation (34)  $T$  goes to infinity, which is impossible in all practical situations. In our calculations  $T$  is chosen so long that the stationary value of  $\langle E_{\text{abs}} \rangle$  is practically achieved. This value is in practice determined by the intensity of the resonant probe field. For probe field intensity of  $75\text{ kWcm}^{-2}$  (i.e.  $10^4$  times weaker than the strong field) the stationary value of  $\langle E_{\text{abs}} \rangle$  is achieved after  $T = 300\text{ ns}$  and for  $75\text{ Wcm}^{-2}$  (i.e.  $10^7$  times weaker than the strong field) after  $T = 10\text{ }\mu\text{s}$ .

It is inherent to the Floquet approximation that the calculation of  $\langle E_{\text{abs}} \rangle$  is performed by matrix-vector multiplications up to times  $T$  in steps of one period  $\tau$  of the Hamiltonian. In our case,  $\tau$  is approximately 30 fs and  $T$  is chosen either 300 ns or  $10\text{ }\mu\text{s}$ , which implies

$10^7$  or  $3 \cdot 10^8$  matrix-vector multiplications, respectively. Although high accuracy is almost always achieved for the numerical integration, after the diagonalisation of the complex evolution matrix  $U$ , severe numerical errors can be introduced in the subsequent time propagation of the initial state; in particular, in our case here, where the diagonalised matrix is used for  $10^7$  or  $3 \cdot 10^8$  sequential matrix-vector operations. For the numerical integration part of the computation, we used the Adams method for the solution of the numerical initial value problem [67] and EISPACK routines [68] for the matrix operations.

In our study, calculations including decay phenomena give the same results as without including any decay. This fact is due to two conditions: Firstly, the states of the ground  $^2P^\circ$  term, between which population transfer occurs due to the resonant probe field, have life-times of the order of ms (see Table 1 in ref. [42]). Such life-times are much longer than the typical time scales considered here. Secondly, the states of the electronically excited configurations, which have life-times of the order of ns according to the Einstein coefficients of Table 2 and thus are within the time scales considered, remain always unpopulated because they are far off-resonant. In Section 4, we present the results from calculations without any decay phenomena included.

## 4. Computational results on the iodine atom in strong laser fields

### 4.1. Survey of the models

Our study is organised in five groups of calculations, as given in Table 3 below. The partitioning in several groups enables us to consider terms coupled by magnetic dipole interaction only, in order to study the influence of the strong field only due to this type of interaction, and we gradually include also electric dipole interactions with other excited states. In addition, partitioning in several groups allows us to check the convergence of our results with respect to the number of states considered. All transition moments used in our calculations are given in the Supplementary material of this paper.

In Table 4 the wavenumbers  $\omega_{kl}^{\text{field}}/2\pi c_0$  for transitions  $|^2P_{3/2}^\circ(F=4)m_F\rangle \rightarrow |^2P_{1/2}^\circ(F'=3)m_{F'}\rangle$  calculated

**Table 3.** Partitions of the terms included in our calculations, number of states and type of dipole interaction(s) between the terms in each partition.

	Terms included	Num. of states	Dipole interaction(s)
Group A	1–2	36	Magnetic
Group B	1–4	72	Magnetic and electric
Group C	1–10	144	Magnetic and electric
Group D	1–10,16–19	240	Magnetic and electric
Group E	1–19	312	Magnetic and electric

within perturbation theory according to Equation (42) are summarised. Since we consider electromagnetic fields polarised along the  $z$ -axis, only  $\Delta m_{FF'} = 0$  transitions are allowed. In the same table, the average shift of the wavenumber for the  $^2P_{3/2}(F=4) \rightarrow ^2P_{1/2}(F=3)$  transition is given, which may be of interest for comparison with the calculated position of the absorption profile of the transition for the case that the individual  $\Delta m = 0$  transitions remain unresolved.

We now focus on some computational details of the numerical simulations with two laser fields. As mentioned above, the numerical integration inherent to the Floquet approximation in order to compute the evolution operator  $\hat{U}$  of the system under consideration is time consuming, since it scales non-linearly with both the number of states included and the required numerical accuracy but this does not cause any serious problems. High numerical accuracy is required in order to obtain a high quality diagonalisation of the complex matrix  $U$  for further use in the computation of the time evolution of the system. In order to quantify the quality of the diagonalisation of the complex matrix  $U$ , the matrix  $(Z \cdot D \cdot Z^T - U)$  is calculated, where  $D$  stands for the diagonal matrix, the diagonal elements of which are the eigenvalues of  $U$ ,  $Z$  is the matrix whose columns are the eigenvectors of  $U$  and  $Z^T$  is its transpose. The largest matrix element of  $(Z \cdot D \cdot Z^T - U)$ , defined here in terms of its absolute value as  $\max_{ij}\{|Z \cdot D \cdot Z^T - U\}_{ij}\}$ , is found and used as a measure for the deviation from an exact diagonalisation, for which it should be zero. Also, the orthogonality of the eigenvectors can be checked by finding the largest matrix element of the  $(Z \cdot Z^T - \mathbf{1})$  matrix,  $\max_{ij}\{|Z \cdot Z^T - \mathbf{1}\}_{ij}\}$ , where for an exact diagonalisation it equals zero, too. Finally, since for the computation of the absorbed energy spectra within the Floquet approximation the necessary quantity is the time averaged absorbed energy  $\langle E_{\text{abs}} \rangle$  as given by Equation (34), we also check the time averaged total population  $\sum_{i=1}^n \langle P_i \rangle$ , where  $n$  stands for the number of states included and  $\langle P_i \rangle$  is the time averaged population of state  $i$ ; this quantity within an accurate computation should always be equal to one. We check the above quantities in order to have a measure for the numerical inaccuracies within the calculation of the system evolution, in addition to the criteria for the numerical integration and complex diagonalisation discussed above.

In Tables 5 and 6, typical values are presented for the quantities introduced above in order to quantify the quality of the numerical treatment for all groups of states for which calculations within the Floquet approximation with two laser fields have been possible. For groups D and E, no such calculations have been performed, since test calculations showed that the numerical inaccuracies

**Table 4.** Wavenumbers for transitions  $|^2P_{3/2}^{\circ}(F=4) m_F\rangle \rightarrow |^2P_{1/2}^{\circ}(F'=3) m_{F'}\rangle$  calculated within perturbation theory for groups of states A, B, C, D and E.

$m_F - m_{F'}$	transition wavenumber in $\text{cm}^{-1}$				
	Group A	Group B	Group C	Group D	Group E
(-3) - (-3)	7 603.138 00	7 603.136 13	7 603.138 85	7 603.139 36	7 603.137 20
(-2) - (-2)	7 603.138 00	7 603.136 13	7 603.138 03	7 603.138 52	7 603.136 48
(-1) - (-1)	7 603.138 00	7 603.136 13	7 603.137 54	7 603.138 02	7 603.136 05
0-0	7 603.138 00	7 603.136 13	7 603.137 38	7 603.137 50	7 603.135 90
1-1	7 603.138 00	7 603.136 13	7 603.137 54	7 603.138 02	7 603.136 05
2-2	7 603.138 00	7 603.136 13	7 603.138 03	7 603.138 52	7 603.136 48
3-3	7 603.138 00	7 603.136 13	7 603.138 85	7 603.139 36	7 603.137 20
$ ^2P_{3/2}^{\circ}(F=4) \rightarrow  ^2P_{1/2}^{\circ}(F'=3)$	average transition wavenumber in $\text{cm}^{-1}$				
	7 603.138 00	7 603.136 13	7 603.138 03	7 603.138 47	7 603.136 48
	average shift of the transition wavenumber in $\text{cm}^{-1}$				
	0.0	-0.001 87	0.000 03	0.000 47	-0.001 52

**Table 5.** Characteristic quantities of the calculations with two laser fields within the Floquet approximation for the case where the probe laser is  $10^4$  times weaker than the strong field.

$n$	accuracy <sup>a</sup>	$\max_{ij} \{[Z \cdot D \cdot Z^T - U]\}$	$\max_{ij} \{[Z \cdot Z^T - \mathbf{1}]\}$	$\sum_{i=1}^n \langle P_i \rangle$	
Group A	36	$10^{-14}$	$< 10^{-4}$	$< 10^{-6}$	1.0000
Group B	72	$10^{-13}$	$< 10^{-3}$	$< 10^{-6}$	1.0002
Group C	144	$10^{-11}$	$< 10^{-2}$	$< 10^{-4}$	1.0000

<sup>a</sup> Accuracy required for the numerical integration.**Table 6.** Characteristic quantities of the calculations with two laser fields within the Floquet approximation for the case where the probe laser is  $10^7$  times weaker than the strong field.

$n$	accuracy <sup>a</sup>	$\max_{ij} \{[Z \cdot D \cdot Z^T - U]\}$	$\max_{ij} \{[Z \cdot Z^T - \mathbf{1}]\}$	$\sum_{i=1}^n \langle P_i \rangle$	
Group A	36	$10^{-13}$	$< 10^{-5}$	$< 10^{-4}$	1.0014
Group B	72	$10^{-13}$	$< 10^{-2}$	$< 10^{-4}$	1.0058
Group C	144	$10^{-9}$	$< 10^{-2}$	$< 10^{-4}$	1.0001

<sup>a</sup> Accuracy required for the numerical integration.

introduced by the diagonalisation of the complex evolution matrix have been too large making any further result unreliable. The numerical integration is the dominant

time consuming part of a calculation within the Floquet approximation.

## 4.2. Results on absorption line shifts and splittings in strong fields

Figure 2 shows the absorption spectrum of the  $|^2P_{3/2}^{\circ}(F=4)\rangle \rightarrow |^2P_{1/2}^{\circ}(F'=3)\rangle$  transition with two laser fields, as well as with the probe laser only, for the group of states A. The strongly off-resonant field has an intensity of  $750 \text{ MWcm}^{-2}$  and the probe field is  $10^4$  times weaker (left panel). The absorption profiles in the case of two laser fields coincide on this scale with the profile, when only the probe laser is considered. In the case of two fields, the absorption profile has a Lorentzian line shape centred at  $7\,603.138\,0008(26) \text{ cm}^{-1}$  and a full width at half maximum (FWHM)  $\tilde{\Gamma}_{\text{FWHM}} = 0.867(5) \cdot 10^{-3} \text{ cm}^{-1}$  (here, the standard deviation for the fitted values to a Lorentzian absorption profile is always given in parenthesis in units of the last significant digit). The maximum value of the time averaged absorbed energy

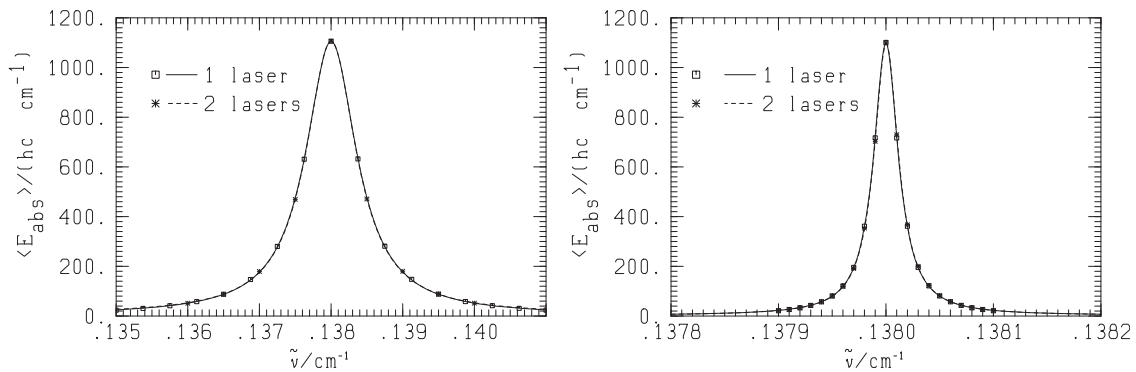


**Figure 2.** The time averaged absorbed energy spectrum of the  $|^2P_{3/2}^{\circ}(F=4)\rangle \rightarrow |^2P_{1/2}^{\circ}(F'=3)\rangle$  transition with two laser fields (dashed line), as well as with the probe laser only (solid line), for the group A of states (see Table 3) are presented. The absorption profile in case of two fields coincides on this scale with the absorption profile, when only the probe laser is considered. The strongly off-resonant field has an intensity of  $750 \text{ MWcm}^{-2}$  and the probe laser is  $10^4$  (left panel) or  $10^7$  (right panel) times weaker. Along the abscissa, only the decimal part of each value is shown, while the integer part is always  $7\,603 \text{ cm}^{-1}$ , i.e.  $\tilde{\nu}_{\text{real}} = \tilde{\nu} + 7\,603 \text{ cm}^{-1}$ . For discussion see text.



$\langle E_{\text{abs}} \rangle$  corresponds to  $1\,104.78(412)\text{ cm}^{-1}$ . The calculated time averaged absorbed energy is consistent with the expected value according to the initial population of the states corresponding to their statistical weights, i.e. each state of the  ${}^2P_{3/2}(F=4)$  hyperfine level has initial population equal to 0.04163. The time averaged absorbed energy due to the seven  $\Delta m = 0$  transitions between the  ${}^2P_{3/2}(F=4)$  and the  ${}^2P_{1/2}(F'=3)$  hyperfine levels is thus expected to be equal to  $1\,107.815\text{ cm}^{-1}$  at  $7\,603.138\text{ cm}^{-1}$ , as irradiation wavenumber. In the case, when only the probe laser is considered, the absorption profile is again a Lorentzian line shape centred at  $7\,603.138\,0004(9)\text{ cm}^{-1}$ , with  $\tilde{\Gamma}_{\text{FWHM}} = 0.873(2) \cdot 10^{-3}\text{ cm}^{-1}$  and a maximum value of  $\langle E_{\text{abs}} \rangle$  corresponding to  $1\,103.86(204)\text{ cm}^{-1}$ .

In the right panel of Figure 2, the calculated absorption profile is shown in the case of excitation with two lasers, as well as with the probe field only, for the same group of states A, but now the probe laser is  $10^7$  times weaker than the strong field. As in the left panel of this figure, the two absorption line shapes are practically indistinguishable on this scale: The Lorentzian line shape with both lasers is centred at  $7\,603.138\,000\,28(3)\text{ cm}^{-1}$ , with  $\tilde{\Gamma}_{\text{FWHM}} = 0.277(1) \cdot 10^{-4}\text{ cm}^{-1}$  and the maximum of  $\langle E_{\text{abs}} \rangle$  corresponds to  $1\,093.85(238)\text{ cm}^{-1}$  and the absorption profile for only the probe laser is centred at  $7\,603.138\,000\,00(3)\text{ cm}^{-1}$ , with  $\tilde{\Gamma}_{\text{FWHM}} = 0.277(1) \cdot 10^{-4}\text{ cm}^{-1}$  and the maximum value of  $\langle E_{\text{abs}} \rangle$  corresponds to  $1\,095.38(253)\text{ cm}^{-1}$ . From the results of Figure 2 it is clear that, for the group of states A where only magnetic dipole interactions in the ground term  ${}^2P^{\circ}$  of atomic iodine are considered, the off-resonant field has no important influence on the position of the  $|{}^2P_{3/2}^{\circ}(F=4) \rightarrow |{}^2P_{1/2}^{\circ}(F'=3) \rangle$  transition, independent on the relative intensity to the probe field. This result obtained by calculating the absorption profiles within the Floquet approximation is in agreement with the result by first order perturbation theory (see Table 4) according to which no shift of the position of the transition under study is expected, when a strongly off-resonant periodic electromagnetic field is present.

The calculated absorption spectra within the group of states B are presented in Figures 3 and 4. Here, in addition to the magnetic dipole interactions in the ground term, the electric dipole interactions of this term with electronically excited states are included. In Figure 3, the absorption spectrum is shown, in the case where the probe field is  $10^4$  times weaker than the strong laser. The Lorentzian line shape for the case when two fields are considered (dashed line) is centred at  $7\,603.136\,1291(8)\text{ cm}^{-1}$ , with  $\tilde{\Gamma}_{\text{FWHM}} = 0.883(2) \cdot 10^{-3}\text{ cm}^{-1}$  and the maximum value of  $\langle E_{\text{abs}} \rangle$  corresponds to  $1\,089.74(212)\text{ cm}^{-1}$ . The Lorentzian line

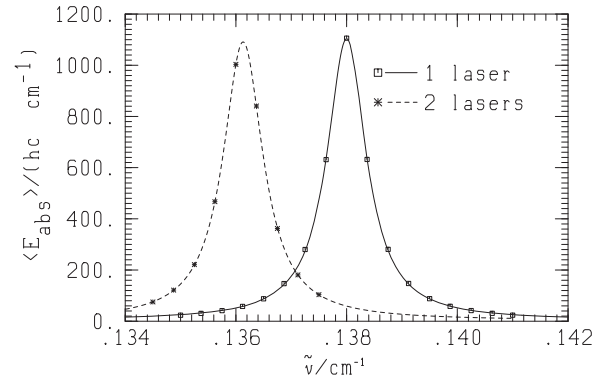


**Figure 3.** The time averaged absorbed energy spectrum of the  $|{}^2P_{3/2}^{\circ}(F=4) \rightarrow |{}^2P_{1/2}^{\circ}(F'=3) \rangle$  transition with two laser fields (dashed line) and with only the probe laser considered (solid line) for the group B of states (see Table 3) are presented. The strongly off-resonant field has an intensity of  $750\text{ MWcm}^{-2}$  and the probe laser is  $10^4$  times weaker. Along the abscissa only the decimal part is shown, while the integer part is always  $7\,603\text{ cm}^{-1}$ , i.e.  $\tilde{\nu}_{\text{real}} = \tilde{\nu} + 7\,603\text{ cm}^{-1}$ . For discussion see text.

shape, when only the probe laser is active (solid line) is symmetric with respect to  $7\,603.138\,0002(17)\text{ cm}^{-1}$ , with  $\tilde{\Gamma}_{\text{FWHM}} = 0.868(4) \cdot 10^{-3}\text{ cm}^{-1}$  and maximum value equal to  $1\,102.05(374)\text{ cm}^{-1}$ . Comparison of the two spectra shows a shift of  $-0.001\,8711(25)\text{ cm}^{-1}$  when the strong laser is present.

Within the group B, the absorption spectrum for the two lasers, when the probe field is  $10^7$  times weaker than the off-resonant field, is shown in Figure 4. It is centred at  $7\,603.13612891(3)\text{ cm}^{-1}$ , with  $\tilde{\Gamma}_{\text{FWHM}} = 0.2780(8) \cdot 10^{-4}\text{ cm}^{-1}$  and a maximum value of  $1\,096.30(178)\text{ cm}^{-1}$ . In the case in which only the probe laser is considered, the centre wavenumber is equal to  $7\,603.138\,000\,00(11)\text{ cm}^{-1}$ , the maximum value of  $\langle E_{\text{abs}} \rangle$  is  $1\,102.52(769)\text{ cm}^{-1}$  and  $\tilde{\Gamma}_{\text{FWHM}}$  equals to  $0.2792(34) \cdot 10^{-4}\text{ cm}^{-1}$ . The shift obtained by comparison of the results in Figure 4 is  $-0.001\,872\,09(14)\text{ cm}^{-1}$ . The above results show that the shift is essentially independent on the relative intensity of the two lasers within the range shown and there is in excellent agreement with the shift calculated with perturbation theory (see Table 4).

The results for group C are shown in Figure 5, where the off-resonant laser is  $10^4$  times stronger than the probe field; the absorption spectrum with both lasers active is shown in this figure. The absorption line is now a superposition of two Lorentzian line shapes. The first peak is centred at  $7\,603.137\,71(2)\text{ cm}^{-1}$  with a  $\tilde{\Gamma}_{\text{FWHM}} = 0.001\,28(5)\text{ cm}^{-1}$  and a maximum value of  $\langle E_{\text{abs}} \rangle / (hc)$  equal to  $650.72\text{ cm}^{-1}$  and the second peak is symmetric with respect to  $7\,603.138\,83(2)\text{ cm}^{-1}$ , with a maximum average absorbed energy corresponding to  $278.31\text{ cm}^{-1}$  and  $\tilde{\Gamma}_{\text{FWHM}} = 0.000\,635(1)\text{ cm}^{-1}$ . In the



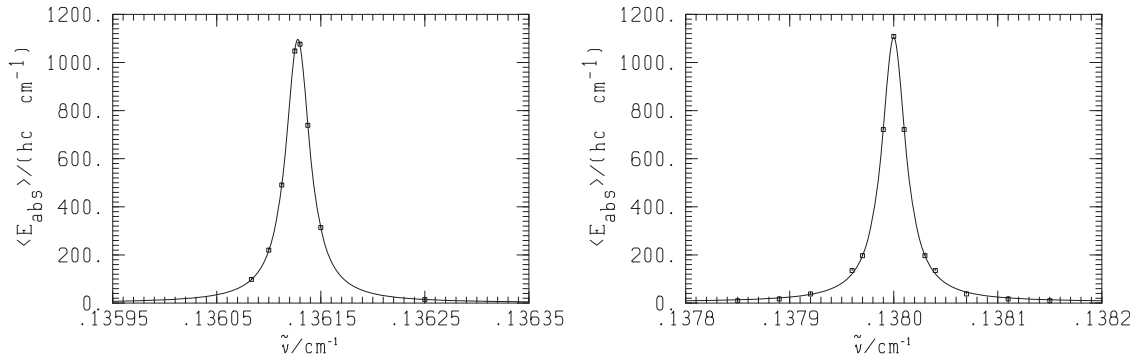


**Figure 4.** Left panel: the time averaged absorbed energy spectrum of the  $|^2P_{3/2}^o(F=4) \rightarrow |^2P_{1/2}^o(F'=3)\rangle$  transition with two laser fields for the group B of states (see Table 3) is presented. The strongly off-resonant field has an intensity of  $750 \text{ MWcm}^{-2}$  and the probe laser is  $10^7$  times weaker. Along the abscissa only the decimal part of each value is shown, while the integer part is always  $7603 \text{ cm}^{-1}$ . Right panel: the time averaged absorbed energy spectrum of the  $|^2P_{3/2}^o(F=4) \rightarrow |^2P_{1/2}^o(F'=3)\rangle$  transition with only the probe laser for the group B of states (see Table 3) is presented. Irradiation intensity as in the left panel. Along the abscissa only the decimal part of each value is shown, while the integer part is always  $7603 \text{ cm}^{-1}$ , i.e.  $\tilde{\nu}_{\text{real}} = \tilde{\nu} + 7603 \text{ cm}^{-1}$ . For discussion see text.

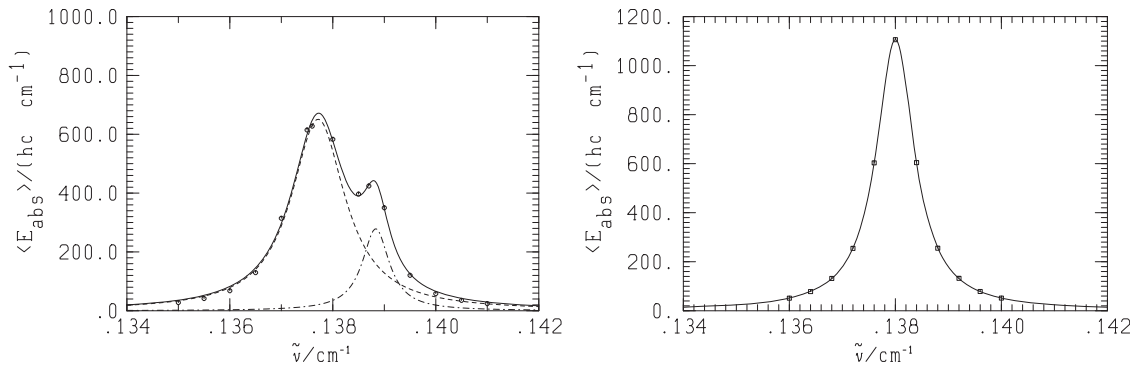


**Figure 5.** Left panel; the time averaged absorbed energy spectrum of the  $|^2P_{3/2}^o(F=4) \rightarrow |^2P_{1/2}^o(F'=3)\rangle$  transition with two laser fields for the group C of states (see Table 3) is presented. The strongly off-resonant field has an intensity of  $750 \text{ MWcm}^{-2}$  and the probe laser is  $10^4$  times weaker. Along the abscissa only the decimal part of each value is shown, while the integer part is always  $7603 \text{ cm}^{-1}$ . Right panel: The time averaged absorbed energy spectrum of the  $|^2P_{3/2}^o(F=4) \rightarrow |^2P_{1/2}^o(F'=3)\rangle$  transition with only the probe laser for the group C of states (see Table 3) is presented. Irradiation conditions as in the left panel. Along the abscissa only the decimal part of each value is shown, while the integer part is always  $7603 \text{ cm}^{-1}$ , i.e.  $\tilde{\nu}_{\text{real}} = \tilde{\nu} + 7603 \text{ cm}^{-1}$ . For discussion see text.

experiment mentioned in the introduction, in which the hyperfine structure of the iodine atom was accurately measured [43,44], the two peaks would be hidden under the Doppler broadening, which is on the order of  $0.01 \text{ cm}^{-1}$  above room temperature as relevant for the kinetic experiments [41–44]; therefore, it is meaningful to calculate an averaged centre of the absorption line by weighting the two centres according to their height. The averaged centre is positioned at  $7603.13805(4) \text{ cm}^{-1}$ , which implies a shift of  $0.00005(4) \text{ cm}^{-1}$  for the position of the transition under study. This value is in excellent agreement with the result by perturbation theory given in Table 4. If only the probe laser is considered the centre wavenumber is  $7603.1380005(5) \text{ cm}^{-1}$ , the  $\tilde{\Gamma}_{\text{FWHM}}$  equals to  $0.000878(1) \text{ cm}^{-1}$  and the maximum value of  $\langle E_{\text{abs}} \rangle / (hc)$  is  $1105.60(112) \text{ cm}^{-1}$ .

In Figure 6, where we show results for group C, the probe laser is  $10^7$  times weaker than the strongly off-resonant field and the substructure hidden previously is now revealed. There are four isolated peaks shown in the main part; three of them are equally high, centred at  $7603.13753000(4)$ ,  $7603.13801000(3)$  and  $7603.13883000(5) \text{ cm}^{-1}$ , with  $\tilde{\Gamma}_{\text{FWHM}} = 0.00003077(5) \text{ cm}^{-1}$ ,  $\tilde{\Gamma}_{\text{FWHM}} = 0.00002806(13) \text{ cm}^{-1}$  and  $\tilde{\Gamma}_{\text{FWHM}} = 0.00002172(13) \text{ cm}^{-1}$  respectively. The maximum values of  $\langle E_{\text{abs}} \rangle$  are almost the same, corresponding to  $324.16 \text{ cm}^{-1}$ ,  $319.42 \text{ cm}^{-1}$  and  $316.39 \text{ cm}^{-1}$ . The smallest peak is centred at  $7603.13737000(4) \text{ cm}^{-1}$ , with  $\tilde{\Gamma}_{\text{FWHM}} = 0.00003167(10) \text{ cm}^{-1}$  and a maximum value  $\langle E_{\text{abs}} \rangle$  corresponding to  $161.04 \text{ cm}^{-1}$ . Comparison with the corresponding results of perturbation theory (Table 4) shows excellent agreement with the calculated

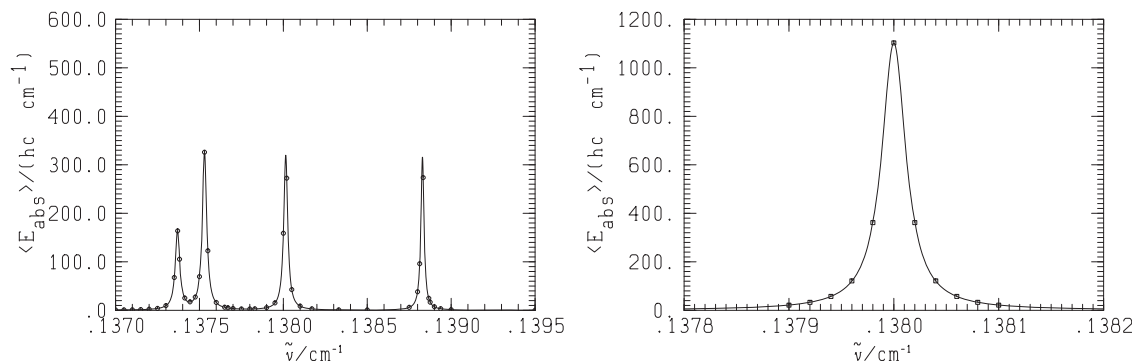


**Figure 6.** Left panel: the time averaged absorbed energy spectrum of the  $|^2P_{3/2}^\circ(F=4)\rangle \rightarrow |^2P_{1/2}^\circ(F'=3)\rangle$  transition with two laser fields for the group C of states (see Table 3) is presented. The strongly off-resonant field has an intensity of  $750 \text{ MWcm}^{-2}$  and the probe laser is  $10^7$  times weaker. Along the abscissa only the decimal part of each value is shown, while the integer part is always  $7\,603 \text{ cm}^{-1}$ . Right panel: The time averaged absorbed energy spectrum of the  $|^2P_{3/2}^\circ(F=4)\rangle \rightarrow |^2P_{1/2}^\circ(F'=3)\rangle$  transition with only the probe laser for the group C of states (see Table 3) is presented. There are no extra lines appearing (also not outside the range shown). Irradiation conditions as in the left panel. Along the abscissa only the decimal part of each value is shown, while the integer part is always  $7\,603 \text{ cm}^{-1}$ , i.e.  $\tilde{\nu}_{\text{real}} = \tilde{\nu} + 7\,603 \text{ cm}^{-1}$ . For discussion see text.

spectra and also helps to identify the corresponding  $|^2P_{3/2}^\circ(F=4)m_F\rangle \rightarrow |^2P_{1/2}^\circ(F'=3)m_{F'}\rangle$  transitions. All transitions with the same absolute value of  $m_F = m_{F'}$  are equally shifted; since there are three pairs of  $m_F = m_{F'}$  values, there are also three equally high peaks. The  $m_F = m_{F'} = 0$  transition has half the height of the other three. The averaged position of the transition calculated within the Floquet approximation is in agreement with the result from the perturbation theory, since all partial results are practically identical for both methods. In the right panel of this figure, the spectrum using only the probe laser is shown, which is centred at  $7\,603.138\,000\,00(2) \text{ cm}^{-1}$ , with  $\tilde{\Gamma}_{\text{FWHM}} = 0.000\,027\,99(3) \text{ cm}^{-1}$  and a maximum value of  $\langle E_{\text{abs}} \rangle$  corresponding to  $1\,102.70(74) \text{ cm}^{-1}$ .

## 5. Discussion and conclusions

The effect of strong off-resonant laser fields on atomic absorption lines probed by weak near-resonant fields is of interest in a variety of experiments. It can play a role in the operation of the iodine atom laser under certain conditions and it is of particular importance for experiments in laser chemical kinetics, where product yields and product state distributions are measured with uncertainty limited simultaneous high time and frequency resolution [41–44], including for instance hyperfine distributions in the iodine atoms. The effects can be estimated easily by perturbation theory [46], but the accuracy of these estimates has to our knowledge not been tested by comparison with accurate numerical calculations. Such a test was the principal goal of the present work.

In summary, the results of the calculations considering two laser fields, one strong off resonant and one weaker

probe field within the Floquet approximation are in excellent agreement with the results obtained with second order perturbation theory for the position of the effective spectral lines of atomic iodine in the presence of a strong off resonant periodic electromagnetic field. Since the treatment within the Floquet approximation allows for ‘multiphoton’ effects of all orders, while only quasi one- and two-photon processes are included in the perturbative treatment, the excellent agreement of the two methods indicates that higher order processes are of no relevance for the observed shift of the transitions under consideration. Moreover, if only the magnetic dipole interactions within the ground term of atomic iodine are considered, no shift of the position of the  $|^2P_{3/2}^\circ(F=4)\rangle \rightarrow |^2P_{1/2}^\circ(F'=3)\rangle$  transition is obtained, indicating that the experimentally obtained shift is due to the coupling of the ground term to electronically excited states, for which the electric dipole type interactions dominate. Surprisingly, adequate spectroscopic information, such as the Einstein coefficients and detailed knowledge of the hyperfine structure for the electronically excited states of atomic iodine, is rare and not well established. Due to this lack of information, it has been practically very difficult to consider a sufficient number of excited states in order to obtain converged results with respect to the number of states included. Therefore, a direct comparison between the theoretical results with the experimentally observed shift is not yet possible. Nevertheless, our results describe semi-quantitatively the observed shifts of the iodine atom under irradiation by two laser fields in agreement with experience in experiments using simultaneous  $\text{CO}_2$  laser excitation, where, however, the Doppler widths are substantially larger than the predicted shifts due to the strong field [41–44]. These Doppler widths are

about  $0.008\text{ cm}^{-1}$  in experiments around room temperature and larger for the more energetic iodine atoms after infrared multiphoton excitation and dissociation of polyatomic iodides [43], where only circumstantial evidence can be seen for the small shifts and splittings with absolute values of about  $0.002\text{ cm}^{-1}$  predicted by the present numerical calculation. These predictions could be tested in high resolution spectroscopic experiments for iodine atoms at low effective temperatures near and below 1 K. Such conditions can be achieved in the spectroscopy of supersonic jet expansions [69,70], which would have to be exposed to the fields from the two lasers as described in the present theoretical work. Both the predicted shifts and splittings would in principle be accessible to such experiments. In the related case of the isoelectronic  $\text{Xe}^+$ , one could consider studying the hyperfine spectra of the isotopes with nuclear spin, characterised already in [71], for instance in experiments with ion traps.

## Acknowledgments

We enjoyed discussions with and help from Georg Seyfang, Csaba Fabri, Frederic Merkt, Eduard Miloglyadov, and Gunther Wichmann. Our work is supported by the Swiss National Science Foundation, an ERC Advanced Grant and by ETH Zurich (in particular the Laboratory of Physical Chemistry). The authors thank also for support from the COST Action CM 1405 (MOLIM), notably to I.T. We enjoyed many years of fruitful interactions with Tim Softley, to whom this paper is dedicated in friendship.

## Disclosure statement

No potential conflict of interest was reported by the authors.

## ORCID

M. Quack  <http://orcid.org/0000-0002-1351-8584>

I. Thanopoulos  <http://orcid.org/0000-0001-8821-8052>

## References

- [1] C. Cohen-Tannoudji, J. Dupont-Roc, and G. Grynberg, *Atom-photon Interactions: Basic Processes and Applications* (John Wiley & Sons, New York, 1992).
- [2] A.D. Bandrauk, *Molecules in Laser Fields* (Dekker, New York, 1994).
- [3] S. Mukamel, *Principles of Nonlinear Optical Spectroscopy* (Oxford University Press, New York, 1995).
- [4] M. Shapiro and P. Brumer, *Principles of Quantum Control of Molecular Processes* (Wiley-Interscience, New York, 2003). "Quantum Control of Molecular Processes" 2nd ed., Wiley-VCH, Weinheim, 2012.
- [5] F. Merkt and M. Quack, Molecular Quantum Mechanics and Molecular Spectra, Molecular Symmetry, and Interaction of Matter with Radiation, in *Handbook of High-resolution Spectroscopy*, edited by M. Quack and F. Merkt (Wiley, Chichester, 2011), Vol. 1, Chap. 1, pp. 1–55.
- [6] W.E. Ernst, T.P. Softley and R.N. Zare, *Phys. Rev. A* **37**, 4172 (1988).
- [7] F. Merkt, R.J. Randall, S.R. Mackenzie and T.P. Softley, *Phys. Rev. Lett.* **76**, 3526 (1996).
- [8] D. Townsend, A.L. Goodgame, S.R. Procter, S.R. Mackenzie and T.P. Softley, *J. Phys. B: At. Mol. Opt. Phys.* **34**, 439 (2001).
- [9] R.A.L. Smith, V.G. Stavros, J.R.R. Verlet, H.H. Fielding, D. Townsend and T.P. Softley, *J. Chem. Phys.* **119**, 3085 (2003).
- [10] E. So, M.T. Bell and T.P. Softley, *Phys. Rev. A* **79**, 012901 (2009).
- [11] W.G. Doherty, M.T. Bell, T.P. Softley, A. Rowland, E. Wrede and D. Carty, *Phys. Chem. Chem. Phys.* **13**, 8441 (2011).
- [12] C.J. Rennick, J. Lam, W.G. Doherty and T.P. Softley, *Phys. Rev. Lett.* **112**, 023002 (2014).
- [13] R.V. Ambartsumian, Y.A. Gorokhov, V.S. Letokhov and G.N. Makarov, *JETP Lett.* **21**, 191 (1975).
- [14] J.L. Lyman, R.J. Jensen, J. Rink, G.P. Robinson and D.S. Rockwood, *Appl. Phys. Lett.* **27**, 87 (1975).
- [15] M.J. Coggiola, P.A. Schulz, Y.T. Lee and Y.R. Shen, *Phys. Rev. Lett.* **38**, 17 (1977).
- [16] E.R. Grant, P.A. Schulz, Aa.S. Subdo, Y.R. Shen and Y.T. Lee, *Phys. Rev. Lett.* **40**, 115 (1978).
- [17] G.J. Diebold, F. Engelke, D.M. Lubman, J.C. Whitehead and R.N. Zare, *J. Chem. Phys.* **67**, 5407 (1977).
- [18] F. Brunner, T.P. Cotter, K.L. Lomba and D. Proch, *J. Chem. Phys.* **67**, 1547 (1977).
- [19] P.A. Schulz, Aa.S. Subdo, D.J. Krajnovich, H.S. Kwok, Y.R. Shen and Y.T. Lee, *Annu. Rev. Phys. Chem.* **30**, 379 (1979).
- [20] Y.T. Lee, *Angew. Chem.* **99**, 967 (1987).
- [21] E. Grunwald, D.F. Denver and P.M. Keehn, *Megawatt Infrared Laser Chemistry* (Wiley, New York, 1978).
- [22] D.W. Lupo and M. Quack, *Chem. Rev.* **87**, 181–216 (1987).
- [23] M. Quack, *Infrared Phys.* **29**, 441–466 (1989).
- [24] M. Quack, *Infrared Phys. Technol.* **36**, 365–380 (1995).
- [25] M. Hippler, M. Quack, R. Schwarz, G. Seyfang, S. Matt, and T. Märk, *Chem. Phys. Lett.* **278**, 111–120 (1997).
- [26] M. Quack, *Chimia* **55**, 753–758 (2001).
- [27] M. Quack, *J. Chem. Phys.* **69** (3), 1282–1307 (1978).
- [28] M. Quack, *Adv. Chem. Phys.* **50**, 395–473 (1982).
- [29] M. Quack, Chapter "Multiphoton Excitation" in *Encyclopedia of Computational Chemistry*, edited by P. von Ragué Schleyer, N. Allinger, T. Clark, J. Gasteiger, P.A. Kollman, H.F. Schaefer III, and P.R. Schreiner (John Wiley and Sons, Chichester, 1998) Vol. 3, pp. 1775–1791.
- [30] M. Quack and E. Sutcliffe, *Chem. Phys. Lett.* **105**, 147–152 (1984).
- [31] K.B. Whaley and J.C. Light, *Phys. Rev. A* **29** (3), 1188–1207 (1984).
- [32] M. Quack and E. Sutcliffe, *J. Chem. Phys.* **83** (8), 3805–3812 (1985).
- [33] M. Quack and E. Sutcliffe, *QCPE Bull.* **6** (3), 98 (1986).
- [34] R. Marquardt and M. Quack, *J. Chem. Phys.* **90** (11), 6320–6327 (1989).
- [35] R. Marquardt and M. Quack, *J. Chem. Phys.* **95** (7), 4854–4867 (1991).
- [36] M. Quack and J. Stohner, *J. Phys. Chem.* **97** (48), 12574–12590 (1993).

- [37] R. Marquardt, M. Quack and I. Thanopoulos, *J. Phys. Chem. A* **104**, 6129–6149 (2000).
- [38] R. Marquardt, M. Quack, I. Thanopoulos and D. Luckhaus, *J. Chem. Phys.* **118**, 643–658 (2003).
- [39] C. Fabri, R. Marquardt, A. Cszaszar and M. Quack, *J. Chem. Phys.* **150**, 014102 (2019).
- [40] A.E. Siegmann, *Lasers* (Oxford University Press, Oxford, 1986).
- [41] Y. He, M. Quack, R. Ranz and G. Seyfang, *Chem. Phys. Lett.* **215** (1,2,3), 228–236 (1993).
- [42] T.-K. Ha, Y. He, J. Pochert, M. Quack, R. Ranz, G. Seyfang and I. Thanopoulos, *Ber. Bunsenges. Phys. Chem.* **99** (3), 384–392 (1995).
- [43] Y. He, J. Pochert, M. Quack, R. Ranz and G. Seyfang, *J. Chem. Soc. Faraday Discuss.* **102**, 275–300 (1995).
- [44] Y. He, J. Pochert, M. Quack, R. Ranz and G. Seyfang, *J. Chem. Soc. Faraday Discuss.* **102**, 354–358 (1995). (replies)
- [45] R.G.W. Norrish, *American Scientist.* **50** (1), 131–157 (1962).
- [46] I. Sobelman, *Atomic Spectra and Radiative Transitions* (Springer-Verlag, Berlin, Heidelberg, New York, 1979).
- [47] M. Fushitani, T. Momose and T. Shida, *Chem. Phys. Lett.* **356**, 375–382 (2002).
- [48] A. Messiah, *Quantum Mechanics*, Vols. 1 and 2 (North-Holland Publishing Company, Amsterdam, 1961).
- [49] R. Marquardt, *Mol. Phys.* (2019). <http://dx.doi.org/10.1080/00268976.2018.1562578>.
- [50] R. Loudon, *The Quantum Theory of Light* (Clarendon Press, Oxford, 1994).
- [51] W. Demtröder, *Laser Spectroscopy*, Springer Series in Chemical Physics, vol. 5 (Springer, Berlin, Heidelberg, New York, 1981).
- [52] M. Quack, Fundamental Symmetries and Symmetry Violations from High-Resolution Spectroscopy in *Handbook of High-resolution Spectroscopy*, edited by M. Quack and F. Merkt (Wiley, Chichester, 2011), Vol. 1, Chap. 18, pp. 659–722.
- [53] M.G. Floquet, *Ann. Scient. Ecole Norm. Sup.* **12** (2), 47 (1883).
- [54] V.I. Arnold, *Gewöhnliche Differentialgleichungen* (Springer-Verlag, Berlin, 1980).
- [55] R.D. Cowan, *The Theory of Atomic Structure and Spectra* (Univ. of Cal. Press, London, 1981).
- [56] K. Blum, *Density Matrix Theory and Applications* (Plenum Press, New York and London, 1981).
- [57] L. Minnhagen, *Ark. Fys.* **21**, 415 (1962).
- [58] K. Murakawa and S. Suwa, *Zeitschrift für Physik* **137**, 575 (1954).
- [59] T. Schmidt, *Zeitschrift für Physik* **112**, 199 (1939).
- [60] C.E. Moore, *National Standard Reference Data Series. National Bureau of Standards (NSRDS-NBS 35)* (US Government Printing Office, Washington, 1971).
- [61] E.U. Condon and G.H. Shortley, *The Theory of Atomic Spectra* (Cambridge University Press, London, 1959).
- [62] A.V. Baklanov, L. Karlsson, B. Lindgren and U. Sassenberg, *J. Phys. B: Atom. Molec. Phys.* **30**, L259 (1997).
- [63] G.M. Lawrence, *Astrophys. J.* **148**, 261 (1967).
- [64] E.R. Cohen, T. Cvitas, J.G. Frey, B. Holnström, K. Kuchitsu, R. Marquardt, I. Mills, F. Pavese, M. Quack, J. Stohner, H.L. Strauss, M. Takami and A. Thor, *Quantities, Units and Symbols in Physical Chemistry*, 3rd ed. (IUPAC and Royal Society of Chemistry, RSC, Cambridge, 2007).
- [65] R.N. Zare, *Angular Momentum, Understanding Spatial Aspects in Chemistry and Physics* (John Wiley & Sons, New York, 1988).
- [66] A. Bauder, Fundamentals of rotational spectroscopy. in *Handbook of High-resolution spectroscopy*, edited by M. Quack and F. Merkt (Wiley, Chichester 2011) Vol. 1, Chap. 2, pp. 57–116.
- [67] C.W. Gear, *Numerical Initial Value Problems in Ordinary Differential Equations* (Prentice-Hall, Englewood Cliffs, 1971).
- [68] B.T. Smith, J.M. Boyle, J.J. Dongarra, B.S. Garbow, Y. Ikebe, V.C. Klema and C.B. Moler, *Lecture Notes in Computer Science: Matrix Eigensystem Routines - EISPACK Guide* (Springer Verlag, Berlin, Heidelberg, Gmbh, 1976).
- [69] M. Snels, V. Horka-Zelenkova, H. Hollenstein and M. Quack, High Resolution FTIR and Diode Laser Spectroscopy of Supersonic Jets, in “Handbook of High-resolution Spectroscopy”, edited by M. Quack and F. Merkt (Wiley, Chichester, 2011), Vol. 2, Chap. 27, pp. 1021–1068.
- [70] M. Hippler, E. Miloglyadov, M. Quack and G. Seyfang, Mass and Isotope Selective Infrared Spectroscopy, in “Handbook of High-Resolution Spectroscopy”, edited by M. Quack and F. Merkt (Wiley, Chichester, 2011), Vol. 2, Chap. 28, pp. 1069–1118.
- [71] M. Schäfer, M. Raunhardt and F. Merkt, *Phys. Rev. A* **81**, 032514 (2010).
- [72] E. Donley, R. Marquardt, M. Quack, J. Stohner, I. Thanopoulos and E.U. Wallenborn, *Mol. Phys.* **99** (15), 1275–1287 (2001). <http://dx.doi.org/10.1080/00268970010009657>.
- [73] R. Prentner, M. Quack, J. Stohner, and M. Willeke, *J. Chem. Phys. A* **119**, 12805–12822 (2015).

## Appendix. Supplementary material

In the supplementary material available, we describe the complete spectroscopic data set as used in the numerical calculations. We also include the FORTRAN code of the URIMIR package, which contains for completeness also the initial parts [33], as these are not any more easily accessible through the QCPE service.

The URIMIR code has the general philosophy of an open source code including as numerical routines also open source programs from various sources as mentioned. It uses only standard FORTRAN language to be easily portable both over time and to various available hardware as recently updated and tested even for the oldest parts. The history of the code is briefly as follows: The earliest programs were written in the context of numerical calculations in refs. [27,28]. These programs were completely rewritten in the context of refs. [30,32] and published by QCPE [33]. The URIMIR package was used to illustrate various examples of multi-photon excitation [72]. Further developments followed as described in refs. [34–38] and finally also in ref. [73], which involved simulations including also the parity violating electroweak interaction.